Research Article Vol. 32, No. 27 / 30 Dec 2024 / Optics Express 47893
Optics EXPRESS

All-reflective freeform microscope objective for ultra-broadband microscopy

Aaron Bauer,[1,2,*] Jannick P. Rolland,[1,2,3] Stephan Clark,[4] Eric Potma,[5] and Adam Hanninen[6]

[1]The Institute of Optics, University of Rochester, Rochester, NY 14627, USA
[2]Center for Freeform Optics, University of Rochester, Rochester, NY 14627, USA
[3]Department of Biomedical Engineering, University of Rochester, Rochester, NY 14627, USA
[4]Clark Optical Consulting and Prototyping, Crowley, TX 76036, USA
[5]Department of Chemistry, University of California, Irvine, Irvine, CA 92697, USA
[6]Trestle Optics, Irvine, CA 92627, USA
[*]aaron.bauer@rochester.edu

Abstract: Conventional refractive microscope objective lenses have limited applicability to a range of imaging modalities due to the dispersive nature of their optical elements. Designing a conventional refractive microscope objective that provides well-corrected imaging over a broad spectral range can be challenging, if not impossible. In contrast, reflective optics are inherently achromatic, so a system composed entirely of reflective elements is free from chromatic aberrations and, as a result, can image over an ultra-wide spectral range with perfect color correction. This study explores the design space of unobscured high numerical aperture, all-reflective microscope objectives. In particular, using freeform optical elements we obviate the need for a center obscuration, rendering the objective's modulation transfer function comparable to that of refractive lens systems of similar numerical aperture. We detail the design process of the reflective objective, from determining the design specifications to the system optimization and sensitivity analysis. The outcome is an all-reflective freeform microscope objective lens with a 0.65 numerical aperture that provides diffraction-limited imaging and is compatible with the geometric constraints of commercial microscope systems.

1. Introduction

Microscopes have long been used to study organisms and structures whose dimensions are beyond the resolution limit of the human eye or a standard camera. Central to the operation of a microscope is its objective lens, which is responsible for generating the first magnified image of the sample under study. Microscopy using conventional refractive microscope objectives has been highly successful for many applications, offering features such as high numerical apertures (NA), wide fields-of-view (FOV), and long working distances (WD). However, designing a high-resolution imaging system that operates over a broad spectral range using conventional refractive elements can be challenging, and in many cases, practically impossible. Conventional microscope objectives are based on refractive materials, which are intrinsically dispersive, and as such, are limited by chromatic aberrations, in particular lateral color [1]. Lens designers attempt to mitigate chromatic aberrations by employing lens elements with different refractive indices, dispersions, and focusing powers, as well as by using cemented doublets and triplets. In this fashion, chromatic aberrations can be reduced but not eliminated. Additionally, there are practical challenges such as identifying materials that are transmissive over multiple wavebands, non-birefringent, and have favorable machining properties. These complications are compounded by the requirement for anti-reflective coatings to cover a broad spectrum. Due to these significant constraints, manufacturers typically design and market refractive-based microscope objectives

#544492 https://doi.org/10.1364/OE.544492
Journal © 2024 Received 10 Oct 2024; revised 3 Dec 2024; accepted 4 Dec 2024; published 16 Dec 2024

Optics EXPRESS

for use within limited spectral ranges, and classify the objectives as either achromatic, which corrects for two specific wavelengths, or apochromatic, which corrects for three wavelengths.

In the biological sciences, microscopists are increasingly adopting multimodal imaging approaches by combining multiple imaging techniques into a single instrument to conduct more thorough sample investigations [2–4]. However, when the chosen modalities involve a broad range of wavelengths, traditional refractive objectives may struggle to provide adequate transmission and imaging quality across the entire spectrum. This challenge is particularly evident in certain imaging modalities, including three-photon excited fluorescence [5–7], third-harmonic generation [8–10], and vibrationally-sensitive sum-frequency generation [11,12], where the excitation and detection wavelengths can be vastly different, presenting difficulties in achieving uniform focusing and efficient light collection across these disparate color regimes. Furthermore, most nonlinear optical imaging techniques require careful management of the lens-induced group delay dispersion for short pulses to maximize signal generation efficiency [13–15].

The challenges associated with transmission and dispersion in traditional objectives underscore the advantages of utilizing an all-reflective microscope objective, which offers ultra-broadband and dispersion-free imaging capabilities. Nonetheless, reflective microscope objectives present their own unique set of design challenges. Most commercially available reflective microscope objectives employ a two-mirror design based on the well-known Schwarzschild telescope [16–19]. While these objectives can provide high NA values in a compact package, they suffer from a major shortcoming – obscuration. The Schwarzschild reflective objectives are rotationally symmetric, resulting in a substantial center obscuration, as evident in the optical layout of an example Schwarzschild objective in Fig. 1. The obscuration reduces the throughput of the system and compromises the imaging performance. For example, a 40% linear central obscuration reduces the transmission throughput by 16% and the modulation transfer function (MTF) by up to 0.24 in the middle spatial frequencies (modulation is measured on a scale from 0 to 1) [20]. The support structures (spider arms) used to hold the central mirror further reduce the MTF by an additional 0.07 and create diffraction artifacts in the image [20]. Given these performance-limiting factors, there is a critical need for an all-reflective solution without obscuration, enabling truly high-resolution, ultra-broadband imaging.

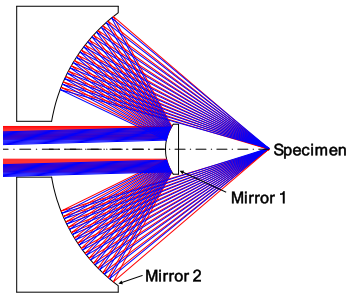

Fig. 1. The optical layout of an all-reflective microscope objective based on the two-mirror Schwarzschild telescope. The edge aperture of Mirror 1 serves as an obscuration that reduces the system throughput and reduces the MTF.

Eliminating the center obscuration in an all-reflective system necessitates breaking the system's symmetry. This can be achieved by tilting each mirror, which redirects the reflected light away from the incoming beam direction, ensuring the subsequent mirrors do not obstruct the light's trajectory. However, this approach introduces a significant challenge as tilting optically powered mirrors generates significant rotationally variant aberrations that elude correction using standard optics. Freeform optics, or optics that have no axes of symmetry either within or outside the aperture of the part [21], are capable of correcting such rotationally variant aberrations while

Optics EXPRESS

maximizing the geometric freedom of the overall folded structure. Freeform optics are not, however, a magic bullet and must be strategically deployed in an optical layout that can fully leverage their aberration correction capabilities [22,23].

Previous work in all-reflective nonlinear optical microscopy has explored the use of spherical mirrors in an off-axis geometry for beam expansion and scan-relay, while still using a commercial rotationally symmetric reflective objective [24,25]. In the area of unobscured reflective microscopes, a 0.4 NA freeform reflective microscope objective was designed to demonstrate a new optical design method for a wide-FOV aplanatic system [26]. An all-reflective design for a complete microscope system with a 0.5 NA objective was studied using freeform surfaces [27]. Finally, a 0.33 NA objective with a strip field was designed leveraging an underlying rotationally symmetric foundation [28].

The work described here expands prior art in two areas – high NA objectives (> 0.60) and compact system volumes. In pursuit of these goals, we will first lay out the system requirements for a high NA, all-reflective microscope objective that is compact enough to be used in a commercial microscope system. We will then describe the optical design process of the objective's front and rear groups. Multiple candidate optical layouts will be presented. Finally, we will compare the two most promising optical layouts via a sensitivity analysis.

2. Specifications of an all-reflective microscope objective for commercial microscope systems

This section defines the critical design parameters and specifications of the unobscured all-reflective microscope objective to be designed in this work. Central to the design criteria is usability across a wide range of microscope systems that are currently commercially available, which places strict limitations on the geometry and size of the optical system. A particularly stringent physical requirement is ensuring the optical axis entering the system is coaxial with the optical axis leaving the system. This constraint may seem trivial (which it is for rotationally symmetric systems), but it dramatically limits the possible selection of unobscured optical layouts. Second, the mechanical length along the input/output axis cannot be too long or the lens will not fit on the objective turret, nor can it be too short as the WD will be too far away from the sample under observation. Lastly, the objective is to be infinity-corrected.

The optical properties of this microscope objective were chosen to provide a high NA over an ultra-broadband spectral range. We chose an NA of 0.65 in air, as this value provides a good balance between a high NA and a design that is feasible to manufacture. At 0.65 NA, the smallest observable feature at 500 nm is about 0.47 μm, which is sufficient to resolve subcellular features, including organelles in microbiology. The nominal designs were optimized at the shortest wavelength in the specified spectral range (500 nm) where the aberration correction required is the most stringent given the linear scaling of wavefront error (WFE) with wavelength. Given the achromatic nature of an all-reflective system, the WFE for the longer wavelengths scales inversely with wavelength. The nominal design aimed to achieve a root-mean-squared (RMS) WFE below 0.035λ at 500 nm across the full field with a maximum distortion below 2%. While ambitious, this provides room for manufacturing tolerances, such that the final "as-built" system is still expected to provide diffraction-limited performance of < 0.07λ RMS at 500 nm.

The full image field is designed to be 300×300 μm^2, which is on par with refractive objectives of similar NA and is a notable improvement over commercial Schwarzschild objectives. Since optical systems scale linearly, the FOV could be expanded by increasing the size of the reflective elements and housing; however, as mentioned, there are competing physical constraints on the optic size for microscope integration. Another design specification that required balancing was the WD, as it is challenging to realize a long WD while maintaining a high NA with unobscured reflective systems. For this system, the WD was set to 2 mm, which, for design purposes, is defined as the axial distance between the image plane and the nearest optical surface.

Optics EXPRESS

The significant advantage of this lens is the broad spectrum that it can accommodate, which is only limited by the spectral reflectivity of the metal used to coat the optical surfaces. Reflective surfaces are agnostic to the wavelength of the incident radiation and will reflect the outgoing radiation at the same angle, providing an extremely broadband transmission range and perfect color correction over the whole FOV regardless of the illumination light source. This system was designed for use from the visible through the mid-infrared spectral ranges, covering over a decade in spectral frequencies (500–6000 nm). For this reason, silver is a good option for the metallic coating. Similar systems designed for applications in the ultraviolet (UV) may use aluminum, and, likewise, systems intended for wavelengths longer than the visible may use gold.

Finally, for many popular imaging modalities, it is essential to have access to the objective's back focal plane (BFP). For example, in differential interference contrast microscopy, the crossover point from the Nomarski (modified Wollaston) prism must coalesce with the lens's BFP. This constraint requires the BFP to be physically located outside or near the back of the lens housing. Similarly, an annular mask may be placed at the BFP for phase-contrast or dark-field microscopy. As an important aside, microscope objectives are designed with the sample under observation at the image plane of the objective, so the common microscopy term "back focal plane" refers to the front focal plane during the design process. Table 1 provides quantitative optical and mechanical design specifications for the all-reflective microscope objective.

Table 1. Specifications for the all-reflective microscope objective

Parameter	Unit	Specification
Wavelength range	nm	500 - 6000
Numerical aperture	-	0.65
Image size	mm	0.3×0.3
Infinite conjugate field of view	deg	3.2×3.2
Working distance	mm	2
Entrance pupil diameter	mm	7
Focal length	mm	5.38
Input/Output optical axis alignment	-	Coaxial
Back focal plane location	-	Accessible
RMS wavefront error	Waves (λ=500 nm)	< 0.035 (nominal) < 0.07 (as-built)
Distortion	%	< 2
System axial length	mm	50 - 70
System half width	mm	< 20 (cylindrical radius) < 12 (one-sided bulge from cylinder)

3. Design strategy

3.1. General system considerations

Given the short system focal length relative to the total optical path, combined with the requirement for large airspaces between the mirrors to facilitate ray clearances, this system needs at least one intermediate image. Further, the last mirror before the image plane requires an extreme curvature to handle the wide angular subtense of the rays in image space due to the system's high NA. That curvature, together with the necessity for system compactness, almost guarantees that the location of the intermediate image will need to be in near proximity to the final mirror. The result is an infinity-corrected objective, with a front group responsible for focusing collimated light to

Optics EXPRESS

an intermediate image plane and a rear group that demagnifies and relays the intermediate image to the final image plane.

3.2. Folding geometry possibilities

As mentioned above, the coaxial alignment requirement for the input and output optical axes severely restricts the available range of folding geometries, and in fact, this constraint necessitates a minimum of four mirrors in the optical layout. The next step in the design process is to identify viable folding geometries and assess their optical and mechanical merits. The possible layouts using four, five, and six mirrors are shown in Fig. 2.

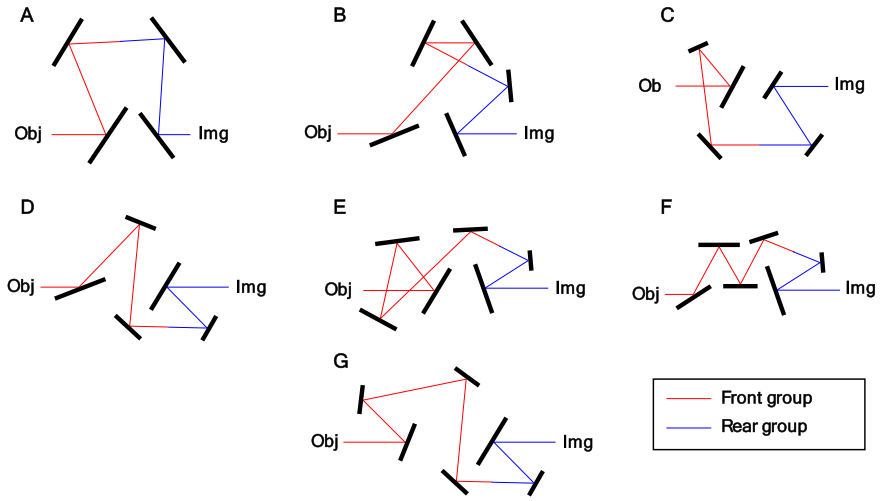

Fig. 2. Sketches of the possible (A) four-mirror, (B-D) five-mirror, and (E-G) six-mirror geometries that provide coaxial object and image planes. To help differentiate between the front and rear groups, the on-axis chief ray is shown as red between the mirrors of the front group and as blue between the mirrors of the rear group for each geometry.

3.3. Geometry down-selection criteria

We are now presented with the possibility of seven geometries for the all-reflective objective. Rather than optimizing each possibility, we will down-select the most promising options based on some selection criteria. By looking at the possibilities in Fig. 2, we can immediately note that the rear group in each geometry option consists of two mirrors prior to the image plane. In each case, the estimated surface locations and tilts appear similar, leading to the conclusion that the rear group will have minimal variability between the different folding geometries. Therefore, we must look at the front group of two, three, or four mirrors to differentiate between the designs.

Given the potentially large number of mirrors used in the geometries above, applying the geometry filtering methods described by Bauer *et al.* [8] to narrow the parameter-space in search for an optimal design becomes impractical. Instead, we look at how the front groups interact with the rear groups and use this information to guide the selection of which layout(s) warrant further optimization. The rear group acts as a finite conjugate relay with a relatively small image size at one conjugate (the final image plane). Therefore, we can approximate these two surfaces as confocal conics, where the final mirror is an elliptical mirror with one of its foci located at the final image plane, which is perfectly imaged to the other ellipse foci (for a point object). The penultimate mirror is a hyperbola with its virtual foci at the aforementioned ellipse foci. The intermediate image for the full system is then at the real foci of the hyperbola. To compensate for

Optics EXPRESS

the aberrations of the extended field beyond a point object of this confocal conic rear group, the two mirrors will soon be given a freeform deviation from the base conics.

Within this framework, the goal of the front group is to image the infinite conjugate object field to the intermediate image plane with as low aberration content as possible to keep the rear group from deviating too far from the confocal conic concept. By conducting a survey of unobscured freeform geometries in the literature utilizing two, three, and four mirrors, we can identify front group configurations that produce an intermediate image of sufficient quality for this task. Specifically, referencing Fig. 2, the front group in Geometry A resembles an off-axis Schwarzschild telescope [29,30], the front group in Geometry B resembles the layout of the optimal two-mirror freeform viewer [31,32] paired with a front fold mirror, and the front group in Geometry E is packaged in the "ball geometry" [33] into which freeform optics were first introduced [34]. The three systems from the literature are shown in Fig. 3. Based on this analysis, we have selected the three geometries A, B, and E for a full system optimization.

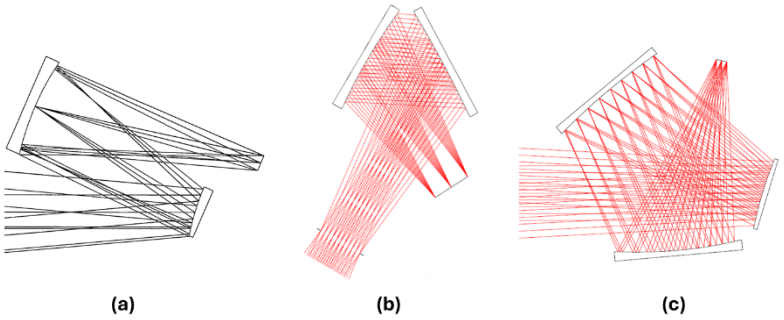

Fig. 3. Unobscured freeform geometries from the literature exhibiting good imaging capabilities that could serve as the front group to the microscope objective. Specifically, Geometry A in Fig. 2 resembles the (a) off-axis Schwarzschild telescope [29,30], Geometry B has the same mirror orientations as (b) the optimal folding geometry for a two-mirror freeform viewfinder [31], and Geometry E has the (c) ball-like layout of the freeform imager [34].

3.4. System optimization

Each of the three selected geometries was given a full system optimization, with the goal of achieving the requisite RMS WFE and package size. The front and rear groups were initially designed as standalone systems – not for performance but to get baseline first-order parameters for each element. The rear group was designed first and was set up as two off-axis conic surfaces (as noted above) at the full NA and image field size. The airspace between the two rear group mirrors, the mirror tilts, and the conic surface shapes were optimized to provide a baseline rear group. From the resulting design of the rear group, an approximate intermediate image size was found that could be used to determine the approximate focal length needed for the front group. Three baseline front groups (one for each geometry) were designed utilizing an aberration-based optimization method whereby the limiting aberrations were evaluated and corrected in a step-by-step process using the corresponding freeform shapes [22]. Care was taken in the design of the front groups to match the ray angles at the intermediate image plane of the rear group to minimize ray errors after combining the two systems. After baseline designs for the front and rear groups were individually designed, each option was merged into a single system by matching the respective intermediate image planes.

In the combined systems, further optimization was performed to enhance the aberration correction and overall structure. In that process, the two mirrors in the rear group were converted

Optics EXPRESS

to freeform surfaces to help reach the performance goals. The freeform surfaces were described by up to 37 Zernike polynomials in the Fringe ordering. While not a focus in the baseline design of each group, constraints on the size of the system were implemented to help meet the packaging requirements. Other design constraints that we implemented included ray clearance constraints, spacing constraints between elements, degeneracy constraints on the freeform terms for the mirrors [35], real-ray distortion constraints, and BFP location constraints. In this way, we were able to fully optimize systems in three different geometries.

4. Design results

4.1. Four-mirror system

As mentioned earlier, a minimum of four mirrors are needed to satisfy the coaxial input/output optical axis constraint. As a point of clarity when discussing the four-mirror system, the first two mirrors in the system are designated as the front group while the last two mirrors are designated as the rear group. The front group takes the general form of an off-axis Schwarzschild telescope. The final design in this layout is shown in Fig. 4 along with its RMS WFE full-field display (FFD). Despite prescribing freeform surfaces to all four mirrors, the nominal system could only achieve near diffraction-limited nominal performance (0.071λ max) at the lower bound of the wavelength range, or 500 nm. The rear group strongly preferred a near telecentric form, which, with an accessible BFP, required the aperture stop to be in object space. The Schwarzschild form performs best in a compact form when the stop is at the secondary mirror; thus, an object space stop deviates from that best form. Also, the system is axially too short for use in commercial microscopes. Due to these limitations, the four-mirror system could not meet the performance and size requirements and will not be considered for the final system.

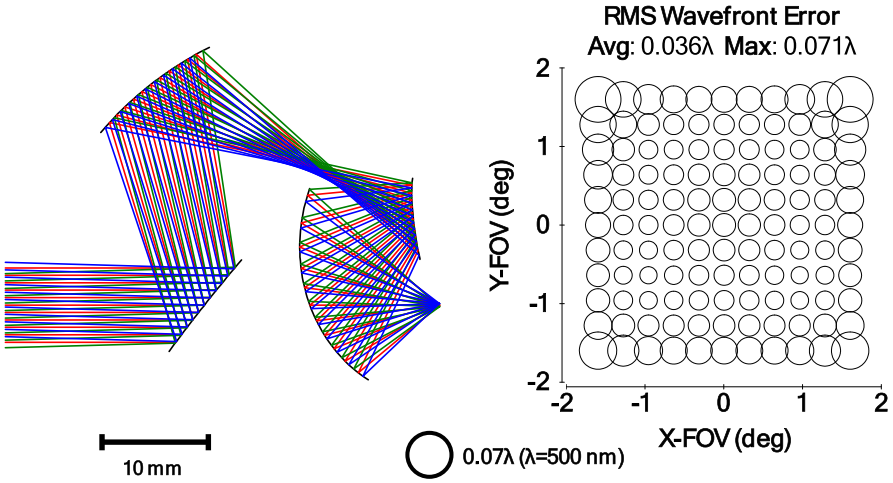

Fig. 4. The final design for the four-mirror system using all freeform mirrors, including an off-axis Schwarzschild-like front group. The FFD shows that its wavefront performance is near the diffraction limit, whereas the nominal requirement is to be far below the diffraction limit.

4.2. Five-mirror system

Incorporating a fifth mirror into the system enhances design flexibility by enabling a three-mirror front group configuration. This front group configuration is derived from the optimal arrangement for a two-mirror freeform imager as shown in Fig. 3(b) [31,32]. To achieve coaxial

Optics EXPRESS

object and image planes while using this mirror configuration, it was necessary to position the two-mirror system away from the common axis, represented as a vertical displacement in Fig. 5. This displacement results in a packaging "bulge" and a non-cylindrical housing geometry to accommodate this mirror positioning. We integrated a fold mirror into the front group as the initial reflective element to direct light rays from input axis to the two-mirror system and then subsequently to the rear group. In our optimized design, all five mirrors feature freeform surfaces, yielding a nominal imaging performance below the diffraction limit. At λ=500 nm, an average RMS WFE of 0.019λ across the entire FOV was achieved. One limitation of the current optimized system is its breach of the minimum system axial length (50 mm) as specified in the requirements table. This could potentially be addressed through further optimization or by including a mechanical extender adjacent to the infinite conjugate side. Overall, this configuration is promising and warrants consideration for the final design.

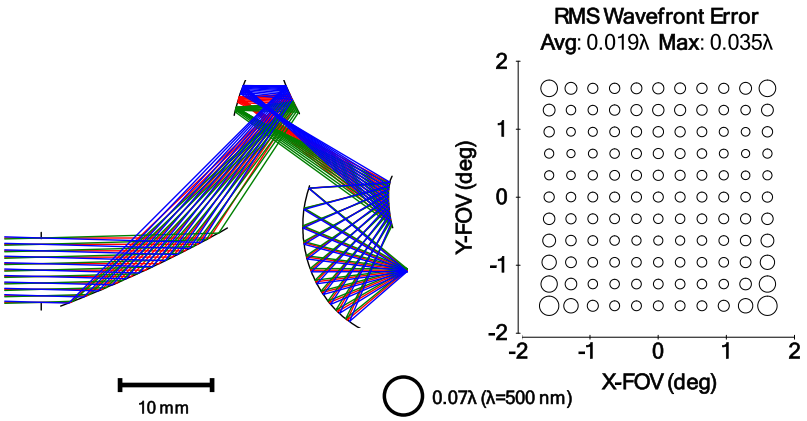

Fig. 5. The final design for the five-mirror system using all freeform mirrors, including a front group that is reminiscent of the optimal two-mirror freeform folding geometry [31]. The maximum nominal RMS WFE is at our goal of 0.035 waves.

4.3. Six-mirror system

The substantial performance enhancements observed with the addition of a fifth mirror to the system naturally lead to an investigation of the potential benefits of incorporating a sixth mirror. In this configuration, the front group is based on the three-mirror freeform imager investigated by Fuerschbach *et al.* [34]. While this front group geometry alone does not direct the light rays into the rear group, the addition of a fold mirror, bringing the total to six mirrors, achieves the desired optical path. The three-mirror imager front group exhibits several advantageous characteristics. First, its extended back focal distance allows for sufficient physical separation between the front and rear groups, ensuring that all components can fit in the housing. Second, the surface curvatures are relatively mild compared to the overall focal length of the system, which is beneficial for sensitivity considerations. Third, it demonstrates inherent high-quality imaging performance with the aperture stop positioned either in object space or at the secondary mirror. The final, all-freeform design in this geometry is shown in Fig. 6. Despite having the most mirrors, this configuration achieves the most compact half width while maintaining a system length that is within the desired range. Moreover, it exhibits superior wavefront performance at 500 nm compared to the previous designs. Given these favorable attributes, this six-mirror system will be considered along with the five-mirror design for the final design.

Optics EXPRESS

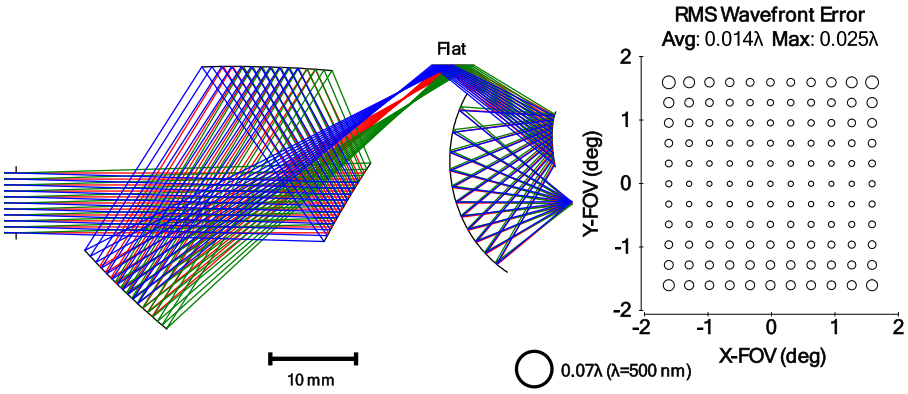

Fig. 6. The final design for the six-mirror system, including a three-mirror freeform front group in a ball geometry [34] and a two-mirror freeform rear group. The flat fold mirror is labeled. This design has the best nominal performance of the three final designs, the smallest half width, and an axial length that fits within the desired range.

5. Sensitivity analysis and design refinement

The five-mirror and six-mirror configurations both exhibit nominal RMS WFE well-below the diffraction limit and have been selected for further analysis and optimization to determine the optimal layout with the best as-built performance. As the nominal designs progress towards fabrication, various analyses must be conducted to predict how the systems will behave post-manufacturing. These analyses include, but are not limited to, tolerance analysis, stray light analysis, and thermal analysis. In this work, we focused specifically on tolerance analysis to differentiate between the design options. Manufacturing imperfections, such as deviations in the shape of optical surfaces and inaccuracies in the final mounting positions of the optics, will affect the as-built performance. By modeling realistic imperfections and assessing their impact on optical performance, we can predict the manufacturing feasibility and sensitivity of each design option. We used the inverse sensitivity mode in the wavefront differential tolerancing routine (TOR) in CODE V to evaluate the sensitivity of each system. In this mode, each defined tolerance is allowed to degrade the performance by a fixed amount – in this case, 0.01λ of RMS WFE. Then, the magnitude of the tolerance that results in that fixed amount of RMS WFE degradation is reported. A more sensitive system will have smaller tolerance values. Our initial focus was on the positioning tolerances for the optical surfaces – X, Y, and Z location and tip, tilt, and clocking rotations of the optical surfaces. Initially, only a focus compensator was used, but due to the fast mirrors used in the rear group it became apparent that an at-assembly push-around compensator would be necessary. Thus, we included the X, Y, and Z positions of one mirror (M4) as compensation in addition to the focus compensator. Figure 7 shows the tolerances that correspond to a 0.01λ RMS WFE decrease. Each cell of the tables is color-coded to indicate the "tightness" of the tolerance where red is the tightest and green is the loosest. This sensitivity "heat-map" reveals that the six-mirror design exhibits overall lower sensitivity. Nonetheless, even its tolerance values are extremely tight, indicating that both designs will incur significant costs to build. This necessitates a refinement of both designs with the objective of reducing their sensitivity to meet looser manufacturing tolerances.

To enhance system robustness and improve tolerance sensitivity, we implemented three strategic approaches. First, instead of aiming for an optimally compact system, we maximized the system dimensions to the allowable limit. Second, we reduced the base curvature of the individual mirrors in the front group while maintaining sufficient RMS WFE. Finally, we employed tolerance-based optimization using CODE V's sensitivity as-built (SAB) optimization. For the five-mirror design,

Optics EXPRESS

	units	M1	M2	M3	M4	M5
X/Y Location	µm	14	9	2	Comp	3
Z Location	µm	12	7	12	Comp	6
Tip/Tilt	min	1.0	0.7	0.3	1.0	0.3
Clocking	min	1.3	3.0	6.7	2.3	0.7

5-Mirror Design

	units	M1	M2	M3	fold	M4	M5
X/Y Location	µm	17	22	17	500	Comp	20
Z Location	µm	31	23	58	16	Comp	21
Tip/Tilt	min	6.7	1.0	0.7	2.0	0.7	0.3
Clocking	min	6.7	1.7	6.7	16.7	1.0	2.0

6-Mirror Design

Fig. 7. The sensitivities of the initial five-mirror and six-mirror designs were evaluated using CODE V's inverse sensitivity tolerancing. Each cell represents the tolerance that degrades the RMS WFE by 0.01λ, where a smaller number indicates higher sensitivity. The cells are color-coded on a spectrum from red to green, where red indicates a higher sensitivity and green indicates a lower sensitivity. Imaging performance is recovered using an at-assembly adjustment of the X/Y/Z position of M4.

the least sensitive version retained freeform surfaces on each mirror. In contrast, the six-mirror configuration allowed for two of the mirrors in the front group to have spherical surface profiles without compromising imaging performance. The layouts for these refined designs are shown in Fig. 8. We again performed an inverse sensitivity analysis using TOR for the refined systems. The results, shown in Fig. 9, again reveal that the six-mirror system exhibits generally lower sensitivity compared to the five-mirror system.

Due to its lower sensitivity to fabrication errors, we further progressed the development of the six-mirror system by switching to sensitivity mode in TOR for tolerance analysis. In this mode, the tolerance values serve as the inputs, and performance changes are generated as the outputs. The modeled tolerances, though stringent, were determined to be feasible with positioning errors in X, Y, and Z of ±25 µm and tip/tilt/clocking errors of ±3 arcmin. The system was also modeled with some baseline figure error tolerances for irregularity (λ/2 IRR) and power (λ/4 DLF). The compensators used in this model included image plane refocus and X/Y/Z/α/β positioning of the penultimate mirror (M4). The results, shown in Fig. 10, indicate the as-built performance will achieve the goal of diffraction-limited imaging with a 98% probability.

As a final comparison, we designed an aspheric Schwarzschild reflective objective with the specifications in Table 1 and a linear obscuration of 40% due to the mirror apertures (no spider arms were modeled here). The MTF of the Schwarzschild system and the refined six-mirror system are shown in Fig. 11. Besides not being diffraction-limited over the full FOV, the effect of the obscuration on the MTF is quite stark, thus emphasizing the importance of developing unobscured solutions. The three freeform mirror shapes for the refined six-mirror design are shown in Fig. 12.

Optics EXPRESS

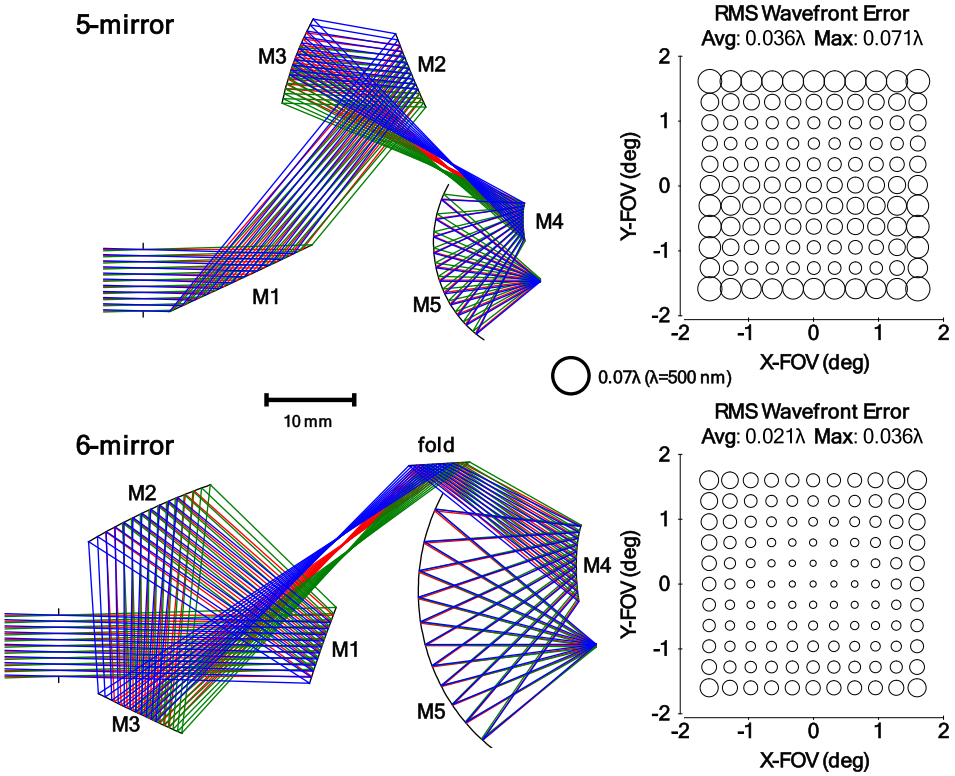

Fig. 8. Refined designs with five and six mirrors. CODE V's SAB optimization was used to lower the sensitivity and the weight on the system volume constraint was reduced. Every mirror in the five-mirror design is freeform. In the six-mirror system, M2, M4, and M5 are freeform, M1 and M3 are spheres, and the fold is flat.

	units	M1	M2	M3	M4	M5
X/Y Location	µm	38	12	8	Comp	10
Z Location	µm	20	54	20	Comp	11
Tip/Tilt	min	1.7	1.7	1.0	1.0	0.7
Clocking	min	6.7	2.7	3.3	2.0	2.0

5-Mirror Refined Design

	units	M1	M2	M3	fold	M4	M5
X/Y Location	µm	225	38	94	500	Comp	30
Z Location	µm	253	62	50	20	Comp	31
Tip/Tilt	min	6.7	1.3	1.0	3.3	0.3	0.3
Clocking	min	16.7	3.3	16.7	16.7	1.0	1.7

6-Mirror Refined Design

Fig. 9. The sensitivity of the refined five-mirror and six-mirror designs was evaluated using CODE V's inverse sensitivity tolerancing. Each table value represents the tolerance that worsens the RMS WFE by 0.01λ, where a larger number indicates lower sensitivity. The cells are color-coded on a spectrum from red to green, where red indicates a higher sensitivity and green indicates a lower sensitivity. Imaging performance is recovered using an at-assembly adjustment of the X/Y/Z position of M4.

Optics EXPRESS

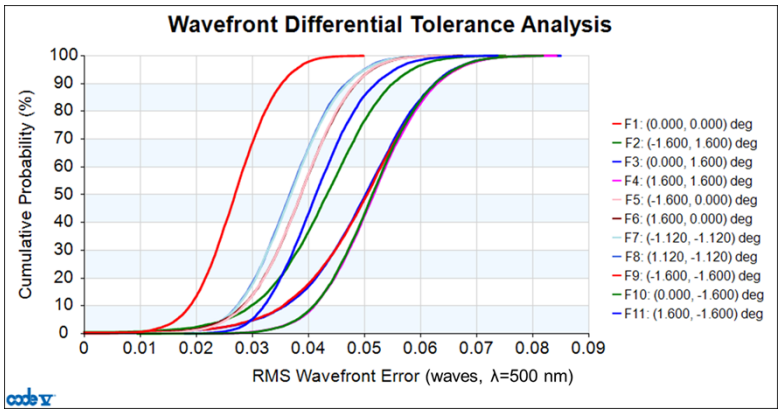

Fig. 10. Manufacturing yield plot for the refined six-mirror design using a set of achievable tolerances: ± 25 μm X/Y/Z mirror positions and ±3 arcmin α/β/γ mirror rotations. Image refocus and the X/Y/Z/α/β positioning of M4 were used as at-assembly compensators. This figure shows a probability of 98% yield of systems with diffraction-limited performance (0.07 waves) or better across the full FOV.

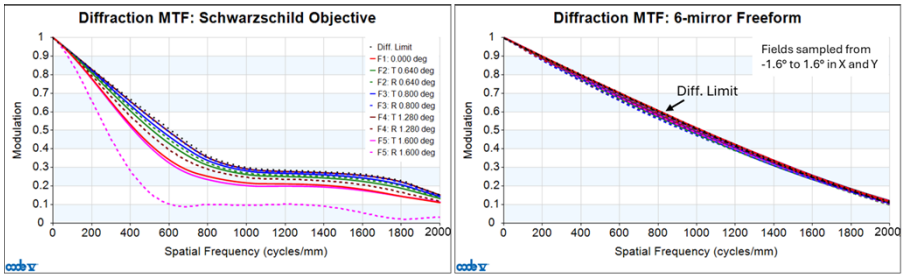

(a) (b)

Fig. 11. MTF plots for the (a) Schwarzschild microscope objective with a 40% linear obscuration due to the mirror apertures and (b) the refined six-mirror freeform unobscured system. The loss of contrast in the middle spatial frequencies of the Schwarzschild objective is noticeable and, further, it is not diffraction-limited over the full FOV.

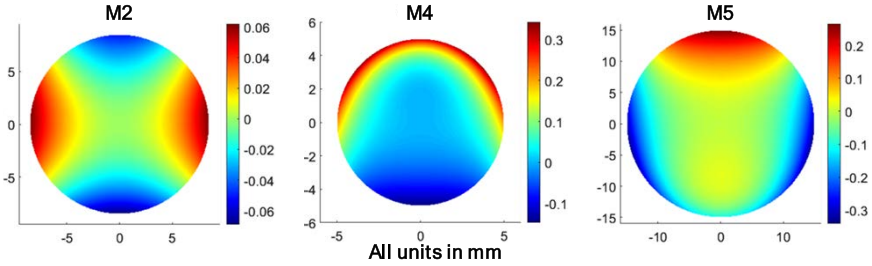

Fig. 12. The departure of the freeform surfaces (M2, M4, and M5) from their best-fit sphere for the refined six-mirror design in Fig. 8. The mirror dimensions and departure values are in mm. The peak-to-valley departures are 0.121 mm, 0.472 mm, and 0.588 mm for M2, M4, and M5, respectively.

Optics EXPRESS

6. Additional microscope geometries

While designing the four-mirror, five-mirror, and six-mirror designs showcased in Section 4, we also explored the potential of geometries with unique characteristics, including the use of double-bounce surfaces where one or more surfaces are used more than once. In general, such a system has the potential to be more compact and less sensitive because the constituent mirrors can be slower as they are used multiple times. The drawback is that the double-bounce surfaces must be tightly constrained to a range of locations/orientations that are conducive to receiving a double-bounce. Although our attention remained with using conventional single-bounce mirror systems for the final design, our investigation yielded several noteworthy double-bounce designs. Figure 13(A) illustrates one such double-bounce system that resembles the six-mirror single-bounce system where the two leftmost mirrors of the front group are used twice. This system met the packaging requirements, but the overall imaging performance was not diffraction-limited at λ=500 nm. Figure 13(B) shows a double-bounce geometry resembling the five-mirror single-bounce system, but where the upper two mirrors of the front group are each used twice. This system had superb optical performance but due to the constraints on the double-bounce surface orientations, the upper two mirrors could not fit within the required packaging. Finally, the five-mirror double-bounce system shown in Fig. 13(C), where the first two mirrors are used twice, met both the packaging and performance requirements and may have some potential to be used in a future objective design. In these designs, all surfaces are designed as freeform surfaces.

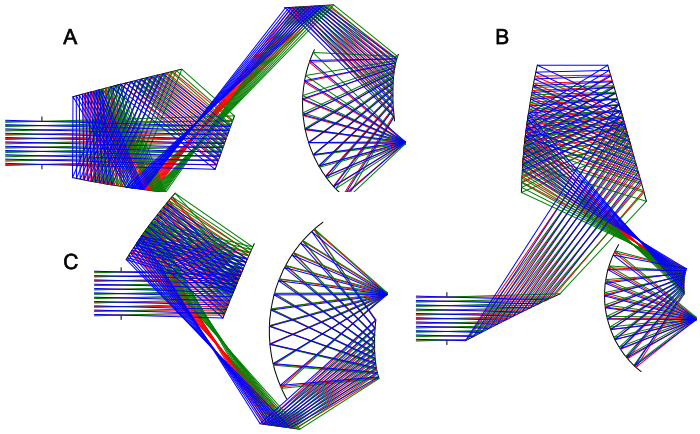

Fig. 13. Various double-bounce geometries were also designed in this study as an interesting aside. They showed some promise for compact geometries and/or diffraction-limited imaging. The (avg/max) RMS WFE of Designs A, B, and C were (0.039λ/0.081λ), (0.010λ/0.018λ), and (0.018λ/0.033λ), respectively, where λ=500 nm.

7. Conclusion

This study presents a methodology for conceptualizing and designing all-reflective freeform microscope objectives compatible with commercial microscope systems that is based on core optical design principles. Our investigation encompassed a systematic exploration of various design configurations, each incorporating a front group with varying mirror quantities and folding geometries. We found that a four-mirror system could not achieve the requisite nominal wavefront performance, and a five-mirror system was prohibitively sensitive. The six-mirror system exhibited the best nominal and as-built imaging performance, while conforming to the dimensional constraints required for use in a commercial microscope system. However, the residual sensitivity of the rear group, impacting the precision needed for the use of M4 as

Optics EXPRESS

compensator, remains a concern and requires additional consideration during the fabrication and assembly plan. Subsequent effort in this area will focus on the opto-mechanical design and assembly strategy. Additional optical design modifications also needed to be address and improve manufacturability, including increasing the WD to allow additional room for mounting the optics, incorporating a coverslip into the design, performing a rigorous surface figure tolerance analysis for the freeform surfaces, and evaluating the required compensation accuracy. These modifications aim to bridge the gap between the theoretical design and a practical implementation, ensuring the viability of the all-reflective microscope objective lens as a tool for a diverse set of imaging applications.

Funding. National Institutes of Health (R43GM149018, R21-EB034084); National Science Foundation (2221721).

Disclosures. SC declares a financial interest in Clark Optical Consulting and AH declares a financial interest in Trestle Optics. All other authors declare no competing interests.

Data availability. Data underlying the results presented in this paper are not publicly available at this time but may be obtained from the authors upon reasonable request.

References

1. J. Bentley and C. Olson, *Field Guide to Lens Design* (SPIE, 2012), pp. 103.
2. S. Yue, M. N. Slipchenko, and J.-X. Cheng, "Multimodal nonlinear optical microscopy," Laser Photonics Rev. **5**(4), 496–512 (2011).
3. J. Rehbinder, L. Brückner, A. Wipfler, *et al.*, "Multimodal nonlinear optical microscopy with shaped 10 fs pulses," Opt. Express **22**(23), 28790–28797 (2014).
4. S. You, H. Tu, E. J. Chaney, *et al.*, "Intravital imaging by simultaneous label-free autofluorescence-multiharmonic microscopy," Nat. Commun. **9**(1), 2125 (2018).
5. S. W. Hell, K. Bahlmann, M. Schrader, *et al.*, "Three-photon excitation in fluorescence microscopy," J. Biomed. Opt. **1**(1), 71–74 (1996).
6. S. Maiti, J. B. Shear, R. M. Williams, *et al.*, "Measuring serotonin distribution in live cells with three-photon excitation," Science **275**(5299), 530–532 (1997).
7. T. Wang and C. Xu, "Three-photon neuronal imaging in deep mouse brain," Optica **7**(8), 947–960 (2020).
8. Y. Barad, H. Eisenberg, M. Horowitz, *et al.*, "Nonlinear scanning laser microscopy by third harmonic generation," Appl. Phys. Lett. **70**(8), 922–924 (1997).
9. M. Müller, J. Squier, K. R. Wilson, *et al.*, "3D microscopy of transparent objects using third-harmonic generation," J. Microsc. **191**(3), 266–274 (1998).
10. D. Débarre, W. Supatto, A.-M. Pena, *et al.*, "Imaging lipid bodies in cells and tissues using third-harmonic generation microscopy," Nat. Methods **3**(1), 47–53 (2006).
11. A. Hanninen, M. W. Shu, and E. O. Potma, "Hyperspectral imaging with laser-scanning sum-frequency generation microscopy," Biomed. Opt. Express **8**(9), 4230–4242 (2017).
12. A. M. Hanninen and E. O. Potma, "Nonlinear optical microscopy with achromatic lenses extending from the visible to the mid-infrared," APL Photonics **4**(8), 080801 (2019).
13. M. Müller, J. Squier, K. R. Wilson, *et al.*, "Dispersion pre-compensation of 15 femtosecond optical pulses for high-numerical-aperture objectives," J. Microsc. **191**(2), 141–150 (1998).
14. V. V. Lozovoy and M. Dantus, "Systematic control of nonlinear optical processes using optimally shaped femtosecond pulses," ChemPhysChem **6**(10), 1970–2000 (2005).
15. N. G. Horton and C. Xu, "Dispersion compensation in three-photon fluorescence microscopy at 1,700 nm," Biomed. Opt. Express **6**(4), 1392–1397 (2015).
16. D. S. Grey and P. H. Lee, "A New series of microscope objectives: I. Catadioptric Newtonian systems*," J. Opt. Soc. Am. **39**(9), 719–722 (1949).
17. D. S. Grey, "A New Series of Microscope Objectives: II. Preliminary Investigation of Catadioptric Schwarzschild Systems*," J. Opt. Soc. Am. **39**(9), 723–728 (1949).
18. K. P. Norris, W. E. Seeds, and M. H. F. Wilkins, "Reflecting microscopes with spherical mirrors," J. Opt. Soc. Am. **41**(2), 111–119 (1951).
19. S. Miyata, S. Yanagawa, and M. Noma, "Reflecting microscope objectives with nonspherical mirrors," J. Opt. Soc. Am. **42**(6), 431_1–432 (1952).
20. J. E. Harvey and C. Ftaclas, "Diffraction effects of telescope secondary mirror spiders on various image-quality criteria," Appl. Opt. **34**(28), 6337–6349 (1995).
21. J. P. Rolland, M. A. Davies, T. J. Suleski, *et al.*, "Freeform optics for imaging," Optica **8**(2), 161–176 (2021).
22. A. Bauer, E. M. Schiesser, and J. P. Rolland, "Starting geometry creation and design method for freeform optics," Nat. Commun. **9**(1), 1756 (2018).
23. A. Bauer, E. M. Schiesser, and J. P. Rolland, "Geometry selection in three-mirror freeform imagers with an accessible exit pupil," Sensors **24**(15), 4816 (2024).

Optics EXPRESS

24. Y. Y. Luna Palacios, S. Khandani, E. P. Garcia, *et al.*, "Spectroscopic analysis of the sum-frequency response of the carbon–hydrogen stretching modes in collagen type I," J. Chem. Phys. **160**(18), 185101 (2024).
25. B. Amirsolaimani, B. Cromey, N. Peyghambarian, *et al.*, "All-reflective multiphoton microscope," Opt. Express **25**(19), 23399–23407 (2017).
26. M. Wang and J. Zhu, "Multi-field cosine condition in the design of wide-field freeform microscope objectives," Opt. Express **31**(26), 43362–43371 (2023).
27. T. Peterson, W. Kang, H. Ma, *et al.*, "All-reflective, unobscured, freeform microscope for biological research: design and fabrication," *Proc. SPIE 12798 International Optical Design Conference* 2023 (2023).
28. M. Wang and J. Zhu, "Off-axis reflective microscope objective with a centimeter scale field of view and micron resolution," Opt. Express **32**(16), 27497–27507 (2024).
29. J. Sasian, "Design of a Schwarzschild flat-field, anastigmatic, unobstructed, wide-field telescope," Opt. Eng. **29**(1), 1 (1990).
30. J. M. Rodgers, "Unobscured mirror designs," *Proc. SPIE 4832, International Optical Design Conference* 2002, 33–60 (2002).
31. A. Bauer and J. P. Rolland, "Design of a freeform electronic viewfinder coupled to aberration fields of freeform optics," Opt. Express **23**(22), 28141–28153 (2015).
32. J. B. Volatier, L. Duveau, and G. Druart, "An exploration of the freeform two-mirror off-axis solution space," JPhys Photonics **2**(1), 014004 (2020).
33. J. M. Rodgers, "Catoptric optical system including concave and convex reflectors," US Patent 5,309,276 (1994).
34. K. Fuerschbach, J. P. Rolland, and K. P. Thompson, "A new family of optical systems employing phi-polynomial surfaces," Opt. Express **19**(22), 21919–21928 (2011).
35. N. Takaki, A. Bauer, and J. P. Rolland, "Degeneracy in freeform surfaces described with orthogonal polynomials," Appl. Opt. **57**(35), 10348–10354 (2018).